Chinese Journal of Natural Medicines

Penicipenoids AG, antioxidant and anti-inflammatory cadinane sesquiterpenoids with rearranged carbon skeletons from the marine sponge symbiotic *Penicillium* sp. 5975

Dongdong Xie, Peihai Li, Lu Zhang, Ruyi Shang, Jiaxin Li, Kechun Liu, Houwen Lin, Shuping Wang, Weihua Jiao

Citation: Dongdong Xie, Peihai Li, Lu Zhang, Ruyi Shang, Jiaxin Li, Kechun Liu, Houwen Lin, Shuping Wang, Weihua Jiao, Penicipenoids AG, antioxidant and anti-inflammatory cadinane sesquiterpenoids with rearranged carbon skeletons from the marine sponge symbiotic *Penicillium* sp. 5975, Chinese Journal of Natural Medicines, 2026, 24(5), 632-640. doi: 10.1016/S1875-5364(26)61181-8.

View online: https://doi.org/10.1016/S1875-5364(26)61181-8

Chinese Journal of Natural Medicines 24 (2026) 632-640

Contents lists available at ScienceDirect

Chinese Journal of Natural Medicines

journal homepage: www.cjnmcpu.com/

Original article

Penicipenoids A–G, antioxidant and anti-inflammatory cadinane sesquiterpenoids with rearranged carbon skeletons from the marine sponge symbiotic *Penicillium* sp. 5975

Dongdong Xie[a,Δ], Peihai Li[b,Δ], Lu Zhang[a], Ruyi Shang[a], Jiaxin Li[a], Kechun Liu[b], Houwen Lin[a], Shuping Wang[a,*], Weihua Jiao[a,*]

[a] *Research Center for Marine Drugs, State Key Laboratory of Microbial Metabolism, Department of Pharmacy, College of Clinical Pharmacy and Ren Ji Hospital, Shanghai Jiao Tong University School of Medicine, Shanghai 200127, China*

[b] *Engineering Research Center of Zebrafish Models for Human Diseases and Drug Screening of Shandong Province, Shandong Provincial Engineering Laboratory for Biological Testing Technology, Key Laboratory for Biosensor of Shandong Province, Biology Institute, Qilu University of Technology (Shandong Academy of Sciences), Jinan 250103, China*

ARTICLE INFO

Article history:
Received 26 June 2025
Revised 4 August 2025
Accepted 13 November 2025
Available online 20 May 2026

Keywords:
Penicillium sp.
Cadinane ses-quiterpenoids
Antioxidant activity
Anti-inflammatory
Rearranged carbon skeleton

ABSTRACT

Seven new sesquiterpenes, named penicipenoids A–G (**1**–**7**), were isolated from rice-based fermentation cultures of the marine sponge-derived fungus *Penicillium* sp. 5975, together with ten known analogues (**8**–**17**). Their structures were elucidated using high-resolution mass spectrometry (HR-MS) and nuclear magnetic resonance (NMR) spectroscopy, supported by single-crystal X-ray diffraction analysis and electronic circular dichroism (ECD) calculations. Penicipenoid A (**1**) features an unprecedented sesquiterpene scaffold characterized by a tricyclo[4.4.$1^{1,6}0^{2,7}$]hendecane core. Penicipenoid D (**4**) contains an unusual furan substructure within the cadinane-type sesquiterpenoid class, while penicipenoid F (**6**) represents a rare norsesquiterpene derivative lacking the carbon atom at the C-7 position. The *in vivo* anti-oxidant and anti-inflammatory effects of these compounds were evaluated using transgenic fluorescent zebrafish models. Penicipenoids A–C (**1**–**3**) exhibited anti-oxidant activity in metronidazole (MTZ)-treated transgenic zebrafish embryos, whereas penicipenoid E (**5**) demonstrated potent anti-inflammatory activity in $CuSO_4$-induced transgenic fluorescent zebrafish embryos.

1. Introduction

Marine sponges are benthic invertebrate metazoans and have been proven to be prolific producers of biologically active natural products [1]. These organisms host diverse microbial communities, including mutualistic, commensal, and parasitic symbionts, which can constitute up to 38% of the total sponge biomass [2]. Sponge-associated fungi have emerged as promising sources of structurally diverse and biologically significant secondary metabolites, such as alkaloids [3, 4], polyketides [5], peptides [6], sesquiterpenoids [7–9], meroterpenoids [10] and others. Among these, sesquiterpenoids exhibit a broad spectrum of biological activities, including anti-inflammatory [7], cytotoxic [11], anti-bacterial [12], antiviral [8], and additional pharmacological effects [13]. Interest in sesquiterpenoids has grown steadily over time, leading to the biosynthesis and chemical synthesis of numerous derivatives for biological evaluation [14, 15].

Previous chemical investigations of sponge-associated fungi have yielded novel bioactive sesquiterpenoids, such as trichodermaloids A–C [16], nigerin, and ochracenes J–L [17]. As part of an ongoing effort to discover new secondary metabolites from marine sponge symbiotic fungi, rice-based fermentation of *Penicillium* sp. 5975, an isolate from the inner tissue of a marine *Dysidea* sp. sponge collected in the South China Sea, yielded an organic extract exhibiting potent *in vitro* anti-oxidant activity at 10 mg·mL^{-1}. Comprehensive chemical analysis of the bioactive extract led to the isolation of seven previously undescribed sesquiterpenoids, named penicipenoids A–G (**1**–**7**), along with ten known analogues (**8**–**17**). Notably, penicipenoid A (**1**) features an unprecedented rearranged cadinane-type sesquiterpene skeleton incorporating a rare tricyclo[4.4.$1^{1,6}0^{2,7}$]hendecane core. Penicipenoid D (**4**) contains an unusual furan substructure, while penicipenoid F (**6**) represents a rare norsesquiterpene within the cadinane sesquiterpenoid family. Bioactivity assessments revealed that penicipenoids A–C and penicipenoid E exhibited dose-dependent anti-oxidant and anti-inflammatory activities, respectively, in *in vivo* transgenic fluorescent zebrafish embryos. Herein, we report the isolation, structural elucidation, and biological evaluation of these newly identified sesquiterpenoids.

2. Results and discussion

Compound **1** was isolated as yellowish needles. The high-resolution electrospray ionization(+) mass spectrometry (HR-ESI(+)-MS) spectrum displayed a protonated ion at *m/z* 265.1435 [M + H]$^+$

* Corresponding author.
E-mail addresses: shupingwang2007@163.com (S. Wang); weihuajiao@hotmail.com (W. Jiao)
Δ These authors contributed equally to this work.

https://doi.org/10.1016/S1875-5364(26)61181-8

(Calcd. for $C_{15}H_{21}O_4$, 265.1434), establishing the molecular formula as $C_{15}H_{20}O_4$ and indicating six double-bond equivalents (DBE). The infrared (IR) spectrum revealed absorption bands corresponding to a hydroxy group at 3414 cm^{-1} and an *α,β*-unsaturated carbonyl group at 1686 cm^{-1} [18, 19]. The ^1H nuclear magnetic resonance (NMR) data for **1** (Tables 1 and S1) exhibited signals attributable to an olefinic methine proton at δ_H 6.29, two methyl doublets at δ_H 0.86 and 0.80, and additional aliphatic methine and methylene protons. The ^{13}C NMR data supported these assignments, showing resonances for one *α,β*-unsaturated ketone at δ_C 203.4, one carbonyl at δ_C 167.8, one nonprotonated olefinic carbon at δ_C 157.4, one olefinic methine carbon at δ_C 128.2, one oxygenated nonprotonated carbon at δ_C 80.3, and two methyl groups at δ_C 21.01 and 20.98, accounting for three of the six DBE and implying the presence of three rings in the structure of **1**. The planar structure of **1** was elucidated using 2D NMR spectra. Heteronuclear multiple bond correlations (HMBCs) of H-2 with C-3, C-4, and C-6; H-4 with C-2, C-3, and C-5; and H-6 with C-1, C-2, C-4, C-5, and C-11 enabled the construction of ring A and placement of the carboxylic acid group at C-5 (Fig. 1 and Table S1). This assignment was further corroborated by HMBCs of H-1 with C-3, C-5, and C-6. Ring B was established through ^1H–^1H correlation spectroscopy (COSY) correlations of H-1/H-10/H_2-9/H_2-8 and HMBCs of H-6/C-7 and C-12, H_2-8/C-7, C-9, C-10, and C-12, and H-1/C-10 and C-13. A hydroxy group and the methylene group CH_2-12 were both assigned to C-7 in ring B based on the downfield chemical shift of C-7 (δ_C 80.3) and HMBCs of H_2-12 with C-6, C-7, and C-8. Additionally, an isopropyl group was positioned at C-10, as indicated by ^1H–^1H COSY correlations of H-10/H-13 and H_3-14/H-13/H_3-15. The diagnostic ^1H–^1H COSY correlation between H-2 and H_2-12, along with HMBCs of H_2-12 with C-1, C-2, and C-3, suggested the formation of a ring C bridging rings A and B. This connectivity was further confirmed by HMBCs of H-1/C-12 and H-2/C-7. Thus, an unprecedented sesquiterpene skeleton featuring a rare tricyclo[4.4.$1^{1,6}0^{2,7}$]hendecane core was established.

The relative configuration of penicipenoid A (**1**) was determined by rotating-frame Overhauser effect spectroscopy (ROESY) analysis (Fig. 2). ROESY correlations between H-6 and H-10 indicated that both protons adopt a *β*-orientation, whereas correlations involving H-12a, H-13, and H-9a suggested an *α*-orientation for these protons. Furthermore, single-crystal X-ray diffraction analysis of **1** using Cu Kα radiation confirmed these assignments and established the absolute configuration as 1*S*,2*S*,6*R*,7*R*,10*R* (Fig. 3), which was consolidated by comparing experimental and calculated ECD spectra [20] of **1** (Supplementary Fig. S11).

HR-ESI(+)-MS analysis of **2** revealed a sodium adduct ion at *m/z* 323.1030 $[M + Na]^+$, corresponding to a molecular formula of $C_{15}H_{21}O_4Cl$ and five DBE. Analysis of the 1D and 2D NMR data for **2** (Tables 1 and S2) indicated the presence of an *α,β*-unsaturated ketone, an *α,β*-unsaturated carboxylic acid, an olefinic methine, and a nonprotonated olefinic carbon, accounting for three DBE

Table 1 ^1H and ^{13}C NMR data for **1**–**4** in DMSO-d_6 [a].

No.	1		2		3		4	
	δ_C mult.	δ_H (*J* in Hz)	δ_C mult.	δ_H (*J* in Hz)	δ_C mult.	δ_H (*J* in Hz)	δ_C mult.	δ_H (*J* in Hz)
1	49.9, CH	2.23, s	37.4, CH	1.92, m	39.5, CH	2.12, m	134.6, C	
2a	48.9, CH	2.52, s	29.7, CH_2	2.85, dd (18.9, 4.2) (*α*)	138.2, CH	6.81, s	120.7, CH	7.71, s
2b				2.11, m (*β*)				
3	203.4, C		149.7, C		128.4, C		134.6, C	
4a	128.2, CH	6.29, s	131.4, CH	6.39, d (2.8)	35.3, CH_2	2.57, m (*α*)	109.8, CH	7.89, s
4b						2.02, m (*β*)		
5	157.4, C		203.1, C		68.5, CH	3.91, m	152.0, C	
6	53.4, CH	2.67, s	57.7, CH	2.61, d (13.3)	52.2, CH	1.61, t (11.2)	130.2, C	
7	80.3, C		72.3, C		73.3, C		121.6, C	
8a	39.7, CH_2	1.73, m	34.3, CH_2	1.23, td (13.3, 3.5)	34.4, CH_2	2.10, m	59.8, CH	5.03, dd (7.2, 3.6)
8b				2.10, m		1.18, m		
9a	25.8, CH_2	1.82, m (*α*)	19.3, CH_2	1.52, m (*α*)	20.5, CH_2	1.55, m	34.8, CH_2	1.98, m (*α*)
9b		1.18, m (*β*)		0.97, dd (12.6, 2.8) (*β*)		0.99, m		1.87, m (*β*)
10	46.1, CH	1.13, m	47.3, CH	1.35, m	45.1, CH	1.18, m	41.0, CH	2.95, q (1.8)
11	167.8, C		167.6, C		167.6, C		168.5, C	
12a	35.0, CH_2	2.02, dd (13.8, 7.8)	48.2, CH_2	3.81, m	49.1, CH_2	4.00, d (11.9)	142.3, CH	7.95, s
12b		1.28, d (13.8)				3.78, d (11.9)		
13	29.6, CH	1.36, m	1.96, m		26.3, CH	2.06, m	29.0, CH	2.14, m
14	21.01[b], CH_3	0.80, d (6.6)	0.73, d (7.0)		15.1, CH_3	0.77, d (7.0)	21.2, CH_3	0.99, d (6.6)
15	20.98[b], CH_3	0.86, d (6.6)	0.92, d (7.0)		21.2, CH_3	0.92, d (7.0)	18.9, CH_3	0.91, d (6.6)
5-OH						6.13, d (3.5)		
7-OH						5.43, s		
11-OH						12.37, s		

[a] ^1H and ^{13}C NMR data respectively recorded in 600 and 150 MHz for **1** and **4** while 700 and 175 MHz for **2** and **3**. [b] overlapping signals.

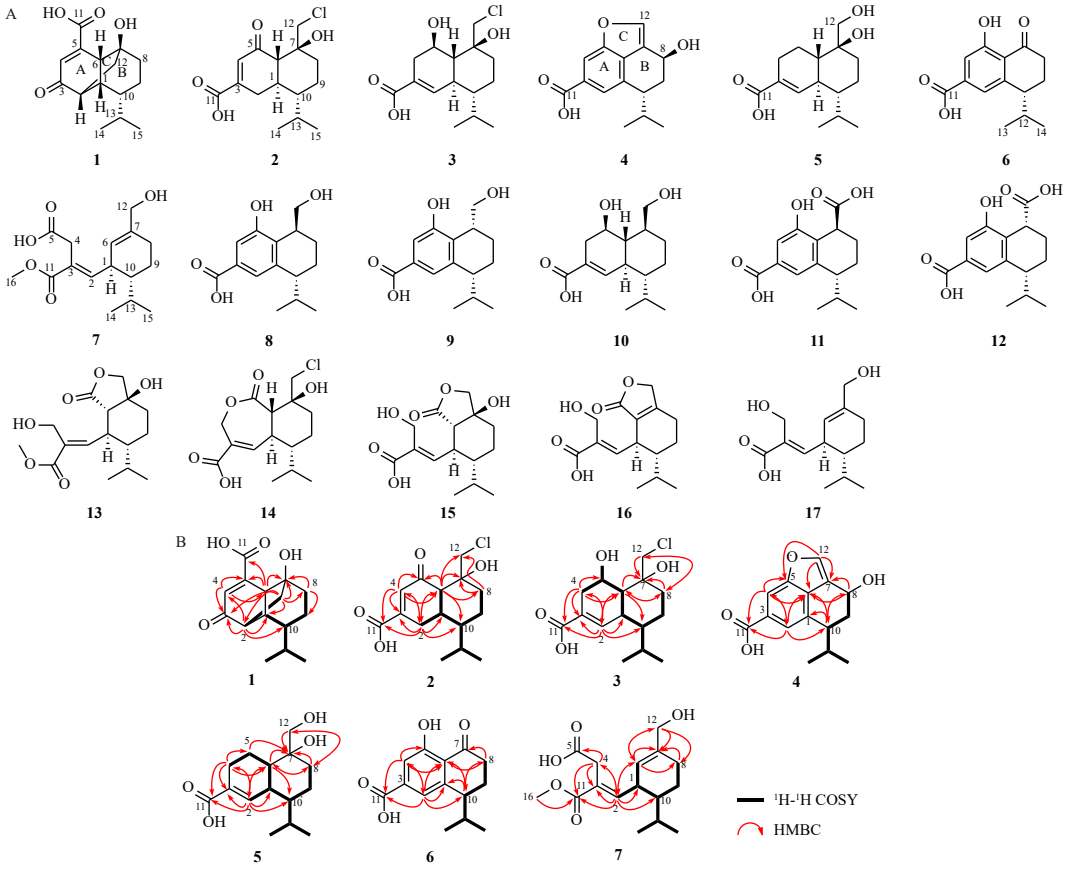

Fig. 1 Chemical strucctures of compounds **1**–**17** (A) and key ^{1}H–^{1}H COSY and HMBC correlations of **1**–**7** (B).

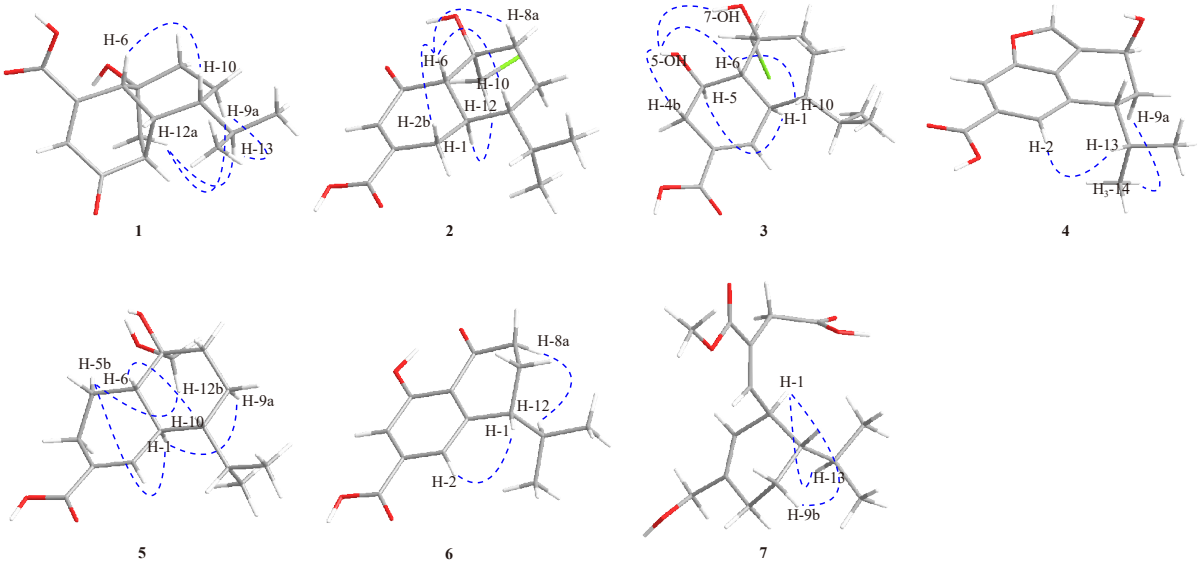

Fig. 2 Key ROESY correlations of **1**–**7**.

and suggesting a bicyclic framework. The ^{1}H–^{1}H COSY correlations of H-2/H-1/H-6, together with HMBCs from H-2 to C-1, C-3, C-4, C-6, and C-11 and from H-6 to C-1, C-2, and C-5, permitted the assembly of ring A and placement of the carboxylic acid at C-3 (Fig. 1). These assignments were further supported by HMBCs of H-4 with C-2, C-3, C-6, and C-11. The ^{1}H–^{1}H COSY correlations of H-1/H-10/H$_2$-9/H$_2$-8 and H$_3$-14/H-13/H-10, combined with HMBCs of H-6 with C-1, C-7, C-8, C-10, and C-12 and H$_2$-8 with C-6, C-7, C-9, C-10, and C-12, indicated the presence of ring B, featuring a chloride-substituted methylene group CH$_2$-12 at C-7 and an isopropyl group at C-10. The latter was further confirmed by HMBCs of H$_2$-12 with C-6, C-7, and C-8. The remaining hydroxy group was assigned to C-7 based on its carbon chemical shift (δ_C 72.3). The large coupling constant of H-6 (J = 13.3 Hz) indicated a *trans*-fusion of rings A and B, consistent with ROESY correlations observed between H-6 and H-10, H-1 and H$_2$-12, and H-1 and H$_3$-14 (Fig. 2). The absolute configuration of penicipenoid B (**2**) was determined to be 1*R*,6*S*,7*S*,10*R* by single-crystal X-ray diffraction (Fig. 3) and confirmed by ECD calculations (Fig. S22).

The HR-ESI(+)-MS spectrum of **3** showed a sodium adduct at

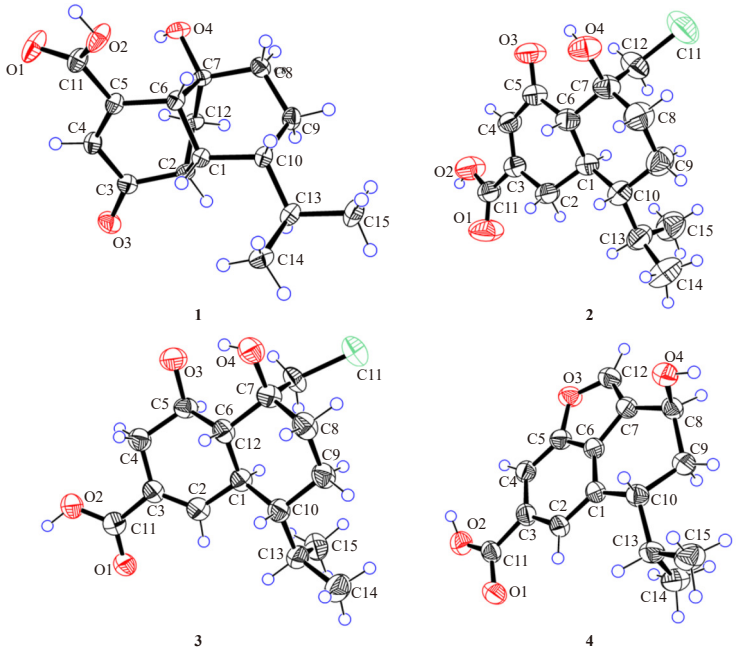

Fig. 3 Single-crystal X-ray diffraction structures of **1**–**4**.

m/z 325.1176 [M + Na]$^+$, consistent with a molecular formula of $C_{15}H_{23}O_4Cl$, representing a homologue of **2** with the addition of a H_2 unit. The ^{1}H and ^{13}C NMR data of **3** (Tables 1 and S3) closely resembled those of **2**, with notable differences: CH_2-2 (δ_C 29.7/δ_H 2.85 and 2.11), CH-4 (δ_C 131.4/δ_H 6.39), and CO-5 (δ_C 203.1) in **2** were replaced by CH-2 (δ_C 138.2/δ_H 6.81), CH_2-4 (δ_C 35.3/δ_H 2.57 and 2.02), and CH(O)-5 (δ_C 68.5/δ_H 3.91) in **3**. This structural assignment was supported by HMBCs of H-2 with C-1, C-3, C-4, C-6, C-10, and C-11, as well as H_2-4 with C-2, C-3, C-5, C-6, and C-11 (Fig. 1). Detailed analysis of ROESY correlations, including H-1/H-5, H-6/H-10, and 5-OH/H-6, established a *trans*-fusion of rings A/B and the *β*-orientation of the 5-OH group. Single-crystal X-ray diffraction analysis assigned the absolute configuration of **3** as 1*R*,5*R*,6*R*,7*S*,10*R* (Fig. 3), which was further corroborated by comparison of the experimental and calculated ECD spectra (Fig. S33).

The HR-ESI(−)-MS spectrum of **4** exhibited a deprotonated ion at *m/z* 259.0993 [M − H]$^-$, consistent with a molecular formula of $C_{15}H_{16}O_4$ and eight DBE. The ^{1}H NMR spectrum of **4** (Tables 1 and S4) displayed three singlet aromatic protons at δ_H 7.71, 7.89, and 7.95, one oxygenated methine proton at δ_H 5.03, and two methyl doublets at δ_H 0.91 and 0.99. The ^{13}C NMR data confirmed these assignments, revealing one carboxylic acid carbon at δ_C 168.7, five nonprotonated aromatic carbons at δ_C 152.0, 134.6, 134.6, 130.2, and 121.6, three aromatic methines at δ_C 120.7, 109.8, and 142.3, one oxygenated aliphatic methine at δ_C 59.8, and two methyl groups at δ_C 18.9 and 21.2, accounting for five of the eight DBE and suggesting three additional rings in **4**. A spin system was identified *via* ^{1}H–^{1}H COSY cross-peaks of H-10/H-13, H_3-14/H-13/H_3-15, and H-10/H_2-9/H-8 (Fig. 1). Three sets of HMBCs, H-2 with C-4, C-6, C-10, and C-11; H-4 with C-5, C-6, and C-11; and H-12 with C-5, C-6, and C-7, enabled the construction of a benzofuran moiety (rings A/C) in **4**. This assignment was reinforced by HMBCs of H-10 with C-1, C-6, and C-8, and H-8 with C-6, C-7, C-9, C-10, and C-12. The relative and absolute configurations of **4** were determined by ROESY and single-crystal X-ray diffraction (Fig. 3). The 8*S*,10*R* configuration was confirmed by ECD calculations (Fig. S44).

HR-ESI(−)-MS analysis of penicipenoid E (**5**) revealed a deprotonated ion at *m/z* 267.1601 [M − H]$^-$, consistent with a molecular formula of $C_{15}H_{24}O_4$, indicating that it is an analogue of **3** in which the chlorine atom is replaced by hydrogen. Comparison of the ^{1}H and ^{13}C NMR data of **5** (Tables 2 and S5) and **3** showed excellent agreement, except for the replacement of CH(O)-5 (δ_C 68.5/δ_H 3.91) and CH_2Cl-12 (δ_C 49.1/δ_H 4.00 and 3.78) in 3 by CH_2-5 (δ_C 21.4/δ_H 2.10 and 1.13) and CH_2OH-12 (δ_C 61.9/δ_H 3.43 and 3.31) in **5**. This assignment was supported by ^{1}H–^{1}H COSY correlations of H_2-4/H_2-5/H-6, along with HMBCs of H-4 with C-2, C-3, C-5, and C-6; H-6 with C-1, C-4, C-5, C-7, and C-12; and H_2-12 with C-6, C-7, and C-8 (Fig. 1). ROESY analysis indicated that **5** shares identical relative configurations at C-1, C-6, C-7, and C-10 with **3** (Fig. 2). The absolute configuration of **5** was assigned as 1*R*,6*S*,7*S*,10*R* based on comparison of the experimental and calculated ECD spectra (Fig. 4).

A deprotonated ion at *m/z* 247.0991 [M − H]$^-$ in the HR-ESI(−)-MS spectrum of **6** indicated a molecular formula of $C_{14}H_{16}O_4$ with seven DBE. The ^{1}H NMR spectrum of **6** (Tables 2 and S6) displayed signals for one phenolic hydroxy proton at δ_H 12.43, two aromatic singlet protons at δ_H 7.29 and 7.19, two methyl doublets at δ_H 0.89 and 0.93, and various aliphatic protons. The ^{13}C NMR data supported these assignments, showing one *α*,*β*-unsaturated ketone at δ_C 205.5, one *α*,*β*-unsaturated carboxylic acid at δ_C 168.0, one phenyl-substituted aromatic carbon at δ_C 161.8, three nonprotonated aromatic carbons at δ_C 147.9, 129.7, and 117.0, two aromatic methine carbons at δ_C 119.9 and 115.4, and two methyl carbons at δ_C 19.7 and 21.4, accounting for five of the seven DBE and suggesting a bicyclic structure. A spin system was established *via* ^{1}H–^{1}H COSY correlations of H_2-8/H_2-9/H-10/H-12 and H_3-13/H-12/H_3-14 (Fig. 1). Four HMBC networks, H-2 with C-1, C-6, C-10, and C-11; H-4 with C-2, C-5, C-6, and C-11; H_2-8 with C-7, C-9, and C-10; and H-10 with C-1, C-2, C-6, C-12, and C-14, enabled the construction of a 6/6-bicyclic substructure, with the carboxylic acid at C-3, the phenolic hydroxy at C-5, and the ketone at C-7. The absolute configuration at C-10 was determined as 10 R by comparison of experimental and calculated ECD spectra (Fig. 4).

HR-ESI(−)-MS spectrum of penicipenoid G (**7**) exhibited a deprotonated ion at *m/z* 295.1572 [M − H]$^-$, consistent with a molecular formula of $C_{16}H_{24}O_5$, suggesting that it is an analogue of the known fungal sesquiterpene trichocitrinovirene A with an additional CH_2 unit [21]. The ^{1}H and ^{13}C NMR data of **7** (Tables 2 and S7) were highly similar to those reported for trichocitrinovirene A, with a key difference being an additional methoxy group (δ_C 52.2/δ_H 3.69). The position of this methoxy group was determ-

Table 2 ^{1}H (600 MHz) and ^{13}C (150 MHz) NMR data for **5**–**7** [a].

No.	**5**		**6**		**7**	
	δ_C mult.	δ_H (J in Hz)	δ_C mult.	δ_H (J in Hz)	δ_C mult.	δ_H (J in Hz)
1	39.9, CH	1.96, m	147.9, C		39.6, CH	3.02, t (10.2)
2a	138.8, CH	6.89, s	119.9, CH	7.29, s	151.5, CH	6.81, d (13.2)
2b						
3	131.5, C		129.7, C		130.1, C	
4a	25.5, CH_2	2.30, dd (13.8, 3.6)	115.4, CH	7.19, s	32.4, CH_2	3.42, d (16.8)
4b		1.95, m				3.38, d (16.8)
5a	21.4, CH_2	2.10, m (β)	161.8, C		174.0, C	
5b		1.13, m (α)				
6	48.0, CH	1.22, m	117.0, C		122.2, CH	5.30, s
7	72.2, C		205.5, C		140.3, C	
8a	35.1, CH_2	2.08, m	34.9, CH_2	2.80, m	25.8, CH_2	2.12, m
8b		1.07, m		2.58, dt (18.0, 5.4)		2.03, m
9a	21.1, CH_2	1.49, m (α)	23.5, CH_2	2.05, m	21.1, CH_2	1.78, m (α)
9b		1.25, m (β)				1.32, m (β)
10	45.5, CH	1.05, m	44.2, CH	2.62, m	45.0, CH	1.36, m
11	168.8, C		168.0, C		171.2, C	
12a	61.9, CH_2	3.43, d (9.6)	29.3, CH	2.00, m	66.9, CH_2	4.01, t (13.2)
12b		3.31, d (9.6)				
13	25.9, CH	2.12, m	21.4, CH_3	0.89, d (6.6)	28.6, CH	1.65, m
14	21.3, CH_3	0.92, d (6.0)	19.7, CH_3	0.93, d (6.6)	21.4, CH_3	0.93, d (6.6)
15	15.2, CH_3	0.77, d (6.0)			16.8, CH_3	0.78, d (6.6)
16					52.2, CH_3	3.69, s
5-OH				12.43, s		

[a] the NMR data of **5** and **6** were measured in DMSO-d_6, but the NMR data of **7** were measured in $CDCl_3$.

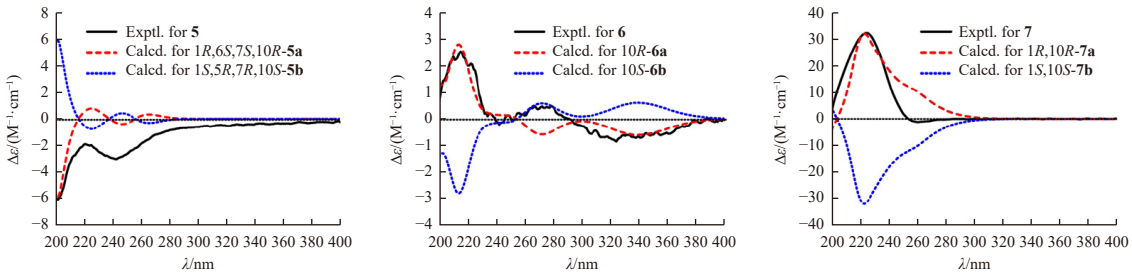

Fig. 4 Comparison of the experimental and calculated ECD spectra of **5**–**7** in MeOH.

ined by HMBCs between H_3-16 and C-11, confirming the attachment of 16-OMe at C-11 (Fig. 1). Comparable ROESY correlations between **7** and trichocitrinovirene A indicated identical relative configurations at the two stereogenic centers (Fig. 2). The absolute configuration of **7** was determined as 1*R*,10*R* by comparison of the experimental and calculated ECD spectra (Fig. 4).

In addition, ten known sesquiterpenes (**8**–**17**) were isolated from the title fungus and identified as aspergilloid G (**8**) [16], aspergilloid H (**9**) [22], rhinomilisin G (**10**) [16], trichodermaloid A (**11**) [16], trichodermaloid B (**12**) [16], methylhydroheptelidate (**13**) [23], heptelidic acid chlorohydrin (**14**) [24], hydroheptelidic acid (**15**) [25], xylaric acid (**16**) [25], and gliocladic acid (**17**) [26] by comparison with previously reported spectroscopic data.

The biosynthetic pathway of penicipenoid A (**1**) is proposed to originate from farnesyl pyrophosphate (FPP), as illustrated in Scheme 1. Cyclization of FPP leads to a cadinene intermediate (**1a**), followed by a cope rearrangement that relocates a methyl group from C-3 to C-5, yielding **1b**. Subsequent oxidation and dehydration steps convert **1b** to **1d**. A Claisen condensation between C-2 and C-12 in **1d** then forms a novel bridged ring beneath the bicyclic system in **1e**. Final oxidation at C-11 affords **1**. To the best of our knowledge, penicipenoid A (**1**) represents the

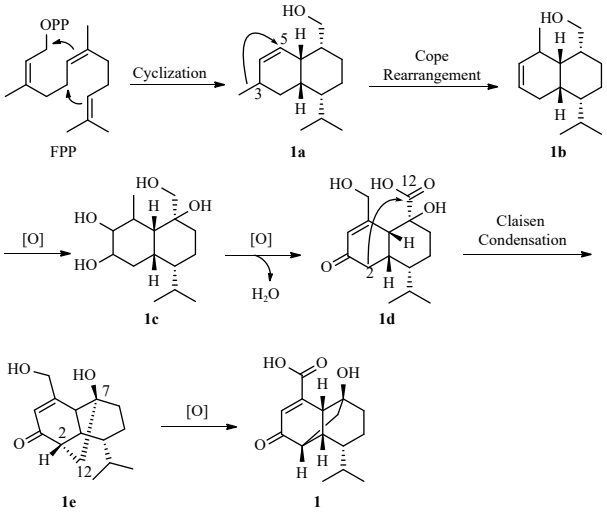

Scheme 1 A plausible biosynthetic pathway for penicipenoid A (**1**).

first naturally occurring rearranged cadinane sesquiterpene featuring the unprecedented tricyclo[4.4.1^{1,6}0^{2,7}]hendecane carbon skeleton.

All 17 isolated sesquiterpenoids (**1**–**17**) were evaluated for anti-oxidant activity using *in vivo* metronidazole (MTZ)-treated transgenic fluorescent zebrafish embryos, with vitamin C as the positive control. Penicipenoids A–C (**1**–**3**) exhibited potent, dose-dependent anti-oxidant activity at concentrations of 10, 20, and 40 μmol·L^{-1} (Fig. 5). Notably, penicipenoid B (**2**) demonstrated greater activity than penicipenoid C (**3**) at 10 and 20 μmol·L^{-1}, despite their structural similarity, except for the presence of an *α,β*-unsaturated ketone at C-5 in **2**. Structure–activity relationship (SAR) analysis suggests that this functional group enhances anti-oxidant activity. However, at 40 μmol·L^{-1}, **2** exhibited reduced activity compared to **3**, likely due to toxicity toward zebrafish embryos not observed with **3**. When anti-inflammatory activity was assessed in $CuSO_4$-induced transgenic zebrafish embryos using indomethacin as the positive control, only penicipenoid E (**5**) showed activity, albeit weaker than the control (Fig. 6). Structural comparison suggests that the two hydroxy groups at C-7 and C-12 may be critical for anti-inflammatory activity among these sesquiterpenes.

3. Conclusion

In conclusion, we report the discovery of seven cadinane sesquiterpenoids with rearranged chemical scaffolds, penicipenoids A–G (**1**–**7**), from the marine sponge symbiotic fungus *Penicillium* sp. 5975. Penicipenoid A (**1**) features an unprecedented sesquiterpene carbon skeleton incorporating a tricyclo[4.4.1^{1,6}0^{2,7}]hendecane core. Penicipenoids A–C (**1**–**3**) exhibited anti-oxidant activity in MTZ-treated transgenic zebrafish embryos, while penicipenoid E (**5**) demonstrated potent anti-inflammatory activity in $CuSO_4$-induced transgenic fluorescent zebrafish embryos. These findings highlight the potential of marine sponge symbiotic fungi as a significant source of bioactive natural products.

4. Experimental

4.1. General experimental procedures

Optical rotations were measured using an Autopol VI Serial #91007 polarimeter (Rudolph Research Analytical, Hackettstown, NJ, USA). UV and ECD spectra were recorded in MeOH on a Jasco J-810 spectropolarimeter. IR spectra were obtained using a VERTEX 70 FT-IR spectrometer (Bruker). HR-ESI-MS and ESI-MS data were acquired on a Thermo Scientific Q Exactive HF-Orbitrap-FTMS and a Waters Xevo G2-SQTOF spectrometer, respectively. One-dimensional (1D) and two-dimensional (2D) NMR experiments were performed on Bruker Avance DRX-600 and 700 MHz NMR spectrometers using DMSO-d_6 (δ_C 39.5/δ_H 2.50) and $CDCl_3$ (δ_C 77.0/δ_H 7.26) as solvents. Semi-preparative high-performance liquid chromatography (HPLC) was conducted on a Waters 1525 binary HPLC pump equipped with a 2998 photodiode array detector. A YMC-Pack Pro RS C_{18} column (250 mm × 10 mm, 5 μm) was used for semi-preparative purification at a flow rate of 2 mL·min^{-1}.

4.2. Collection and isolation of *Penicillium sp. 5975*

The fungal strain *Penicillium* sp. 5975 was isolated from the marine sponge *Dysidea* sp. collected in the South China Sea. The

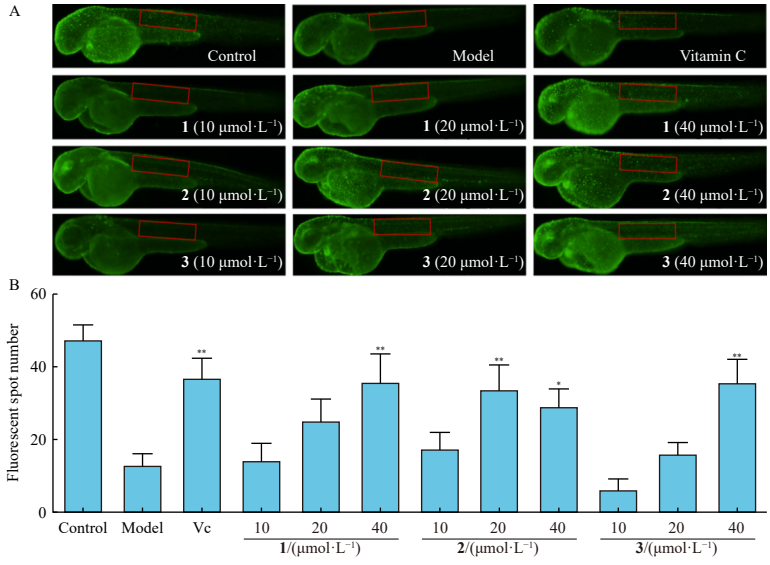

Fig. 5 *In vivo* antioxidant activity of penicipenoids A–C (**1**–**3**) in metronidazole (MTZ)-treatment zebrafish embryos (n = 5). (A) *In vivo* visualization of Tg (*krt4:NTR-hKikGR*)^{cy17} zebrafish skin fluorescence treated with different concentrations (10, 20, and 40 μmol·L^{-1}) of **1**–**3**, using vitamin C as positive control. (B) Quantitative analysis of fluorescence spots (FS) in zebrafish (in the red frame) treated with **1**–**3**. Data were derived from the five independent experiments and represented as mean ± SD. $^{*}P$ < 0.05, $^{**}P$ < 0.01 *vs* model.

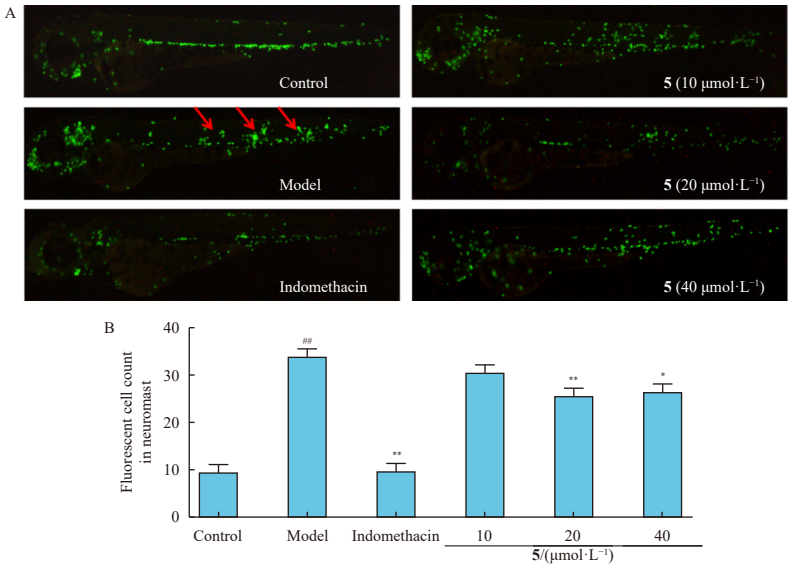

Fig. 6 *In vivo* anti-inflammatory activity of penicipenoid E (5) in zebrafish embryos (n = 5). (A) Images of inflammatory sites in $CuSO_4$-induced transgenic fluorescent zebrafish (Tg:zlyz-EGFP) expressing enhanced green fluorescent protein (EGFP) treated with different concentrations (10, 20, and 40 μmol·L^{-1}) of **5**, using indomethacin as positive control. (B) Quantitative analysis of macrophages in the region of inflammatory sites in zebrafish treated with **5**. Data were derived from the three independent experiments and represented as mean ± SD. $^{*}P < 0.05$, $^{**}P < 0.01$ *vs* model.

fungus was cultured on ISP2 medium at 30 °C for three days to prepare genomic deoxyribonucleic acid (DNA), which was extracted using a commercial DNA kit (DNA-Technology Ltd.) following the manufacturer's instructions. The 18S ribosomal ribonucleic acid (rRNA) gene was amplified *via* PCR using universal primers 3NDF (5′-GGCAAGTCTGGTGCCAG-3′) and V4_euk_R2 (5′-ACGGTATCTATCTCTTCG-3′). BLAST analysis revealed that the amplified small subunit rRNA gene sequence (ID: PV211015) shares 99% homology with other members of the genus *Penicillium* sp. (Supporting Information). The strain is preserved at the Research Center for Marine Drugs, Ren Ji Hospital, Shanghai Jiao Tong University School of Medicine, Shanghai, China.

4.3. Cultivation and isolation of Penicillium sp. 5975

Penicillium sp. was cultivated on rice medium at room temperature for 30 days in 50 Erlenmeyer flasks, each containing 70 g of rice, 0.3 g of peptone, 0.3 g of yeast extract, 0.1 g of monosodium glutamate, and 0.3 g of NaCl. The fermented culture was exhaustively extracted with EtOAc until the organic phase became nearly colorless. The combined EtOAc extracts were concentrated in vacuo to afford a crude extract (97 g), which was sequentially partitioned between H_2O and equal volumes of EtOAc. The dried EtOAc-soluble fraction (40 g) was subjected to silica gel column chromatography eluted with a gradient of EtOAc in petroleum ether to yield 13 fractions (E1–E13). Fractions E4–E8 were combined into a single fraction (E48, 3.0 g), which was further separated by normal -phase silica MPLC (gradient petroleum ether/EtOAc) to give ten subfractions (E48A–E48J). Subfraction E48C (36.9 mg) was purified by reversed-phase (RP) semi-preparative HPLC (30% MeCN/H_2O) to yield aspergilloid G (**8**, 2.8 mg) and aspergilloid H (**9**, 5.8 mg). Subfraction E48G (45.7 mg) was purified under the same conditions (25% MeCN/H_2O) to afford penicipenoid E (**5**, 3.8 mg) and methylhydroheptelidate (**13**, 5.2 mg). Subfraction E48K (21.0 mg) was purified by RP semi-prep HPLC (35% MeCN/H_2O) to yield penicipenoid C (**3**, 10.2 mg). Fraction E9 (631 mg) was separated by RP C_{18}-MPLC (gradient MeCN/H_2O, 10%–100%) to afford five subfractions (E9A–E9E). Subfraction E9C (84.9 mg) was further purified by RP semi-prep HPLC (20% MeCN/H_2O) to yield rhinomilisin G (**10**, 7.0 mg). Fraction E10 (2.2 g) was similarly separated by RP C_{18}-MPLC (10%–100% MeCN/H_2O) to yield five subfractions (E10A–E10E). Subfraction E10D (85.7 mg) was purified by RP semi-prep HPLC (30% MeCN/H_2O) to afford penicipenoid A (**1**, 5.2 mg), trichodermaloid A (**11**, 4.8 mg), and trichodermaloid B (**12**, 7.3 mg). Fraction E11 (2.5 g) was subjected to RP C_{18}-MPLC (10%–100% MeCN/H_2O) to afford six subfractions (E11A–E11F). Subfraction E11B (71.3 mg) was purified by RP semi-prep HPLC (35% MeCN/H_2O) to yield penicipenoid B (**2**, 7.1 mg). Fractions E12 and E13 were combined into a new fraction (E1213, 4.1 g), which was separated by RP C_{18}-MPLC (10%–100%) to afford 22 subfractions (E1213A–E1213V). Subfraction E1213A (101.6 mg) was purified by RP semi-prep HPLC (20% MeCN/H_2O) to yield penicipenoid D (**4**, 5.8 mg), heptelidic acid chlorohydrin (**14**, 8.9 mg), xylaric acid (**16**, 2.7 mg), and gliocablic acid (**17**, 3.3 mg). Subfraction E1213M (21.9 mg) was separated by RP semi-prep HPLC (60% MeOH/H_2O) to afford hydroheptelidic acid (**15**, 4.0 mg). Subfraction E1213N (91.5 mg) was purified by RP semi-prep HPLC (30% MeCN/H_2O) to afford penicipenoid F (**6**, 2.5 mg) and penicipenoid G (**7**, 2.0 mg).

Penicipenoid A (**1**): yellowish needles; $[\alpha]_D^{25}$ +172.1 (c 0.24, MeOH); UV (MeOH) λ_{max} (logε): 200 (2.60) nm; ECD (c 9.0 × 10^{-4} mol·L^{-1}, MeOH) λ_{max} ($\Delta\varepsilon$) 227 (−16.7), 265 (+17.8) nm; IR (KBr) ν_{max}: 3414, 2960, 2871, 1686, 1470, 1387, 1339, 1250, 1098, 1065, 999, 950, 720, 692 cm^{-1}; ^{1}H (600 MHz, DMSO-d_6) and ^{13}C (150 MHz, DMSO-d_6) NMR, Tables 1 and S1; ESI-MS m/z 265.1 [M + H]$^+$; HR-ESI(+)-MS m/z 265.1435 [M + H]$^+$ (Calcd. for $C_{15}H_{21}O_4$, 265.1434).

Penicipenoid B (**2**): colorless needles; $[\alpha]_D^{25}$ +41.7 (c 0.41, MeOH); UV (MeOH) λ_{max} (logε): 238 (3.62) nm; ECD (c 1.67 × 10^{-4} mol·L^{-1}, MeOH) λ_{max} ($\Delta\varepsilon$) 211 (+15.0) nm; IR (KBr) ν_{max}: 2959, 1720, 1660, 1462, 1452, 1389, 1370, 1344, 1238, 1204, 1084, 1060, 1024, 993, 806, 747, 702 cm^{-1}; ^{1}H (700 MHz, DMSO-d_6) and ^{13}C (175 MHz, DMSO-d_6) NMR, Tables 1 and S2; ESI-MS m/z 323.1 [M + Na]$^+$; HR-ESI(+)-MS m/z 323.1030 [M + Na]$^+$ (Calcd. for $C_{15}H_{21}O_4ClNa$, 323.1030).

Penicipenoid C (**3**): colorless needles; $[\alpha]_D^{25}$ −9.6 (c 0.25, MeOH); UV (MeOH) λ_{max} (logε): 218 (3.92) nm; ECD (c 1.66 × 10^{-4} mol·L^{-1}, MeOH) λ_{max} ($\Delta\varepsilon$) 200 (−14.2), 244 (−5.13) nm; IR (KBr) ν_{max}: 3399, 2960, 2873, 2630, 1686, 1644, 1422, 1388, 1267, 1120, 1092, 1078, 1011, 998, 917, 876, 787, 745 cm^{-1}; ^{1}H (700 MHz, DMSO-d_6) and ^{13}C (175 MHz, DMSO-d_6) NMR, Tables 1 and S3; ESI-MS m/z 325.1 [M + Na]$^+$; HR-ESI(+)-MS m/z 325.1176 [M + Na]$^+$ (Calcd. for $C_{15}H_{23}O_4ClNa$, 325.1177).

Penicipenoid D (**4**): red needles; $[\alpha]_D^{25}$ +12.0 (*c* 0.58, MeOH); UV (MeOH) λ_{max} (logε): 223 (3.39), 273 (3.41) nm; ECD (*c* 1.93 × 10^{-4} mol·L^{-1}, MeOH) λ_{max} ($\Delta\varepsilon$) 225 (+9.1), 272 (−3.29) nm; IR (KBr) ν_{max}: 3305, 2959, 2929, 1691, 1606, 1573, 1417, 1293, 1243, 1115, 1063, 1004, 934, 780 cm^{-1}; ^1H (600 MHz, DMSO-d_6) and ^{13}C (150 MHz, DMSO-d_6) NMR, Tables 1 and S4; ESI-MS *m/z* 259.1 [M − H]$^-$; HR-ESI(−)-MS *m/z* 259.0993 [M − H]$^-$ (Calcd. for $C_{15}H_{15}O_4$, 259.0976).

Penicipenoid E (**5**): white amorphous solids; $[\alpha]_D^{25}$ +3.4 (*c* 0.74, MeOH); UV (MeOH) λ_{max} (logε): 213 (3.69) nm; ECD (*c* 1.88 × 10^{-4} mol·L^{-1}, MeOH) λ_{max} ($\Delta\varepsilon$) 202 (−6.1), 243 (−3.03) nm; IR (KBr) ν_{max}: 3374, 2955, 2869, 1687, 1641, 1536, 1463, 1402, 1369, 1260, 1080, 1047, 1009, 914, 756 cm^{-1}; ^1H (600 MHz, DMSO-d_6) and ^{13}C (150 MHz, DMSO-d_6) NMR, Tables 2 and S5; ESI-MS *m/z* 267.1 [M − H]$^-$; HR-ESI(−)-MS *m/z* 267.1601 [M − H]$^-$ (Calcd. for $C_{15}H_{23}O_4$, 267.1602).

Penicipenoid F (**6**): colorless amorphous solids; $[\alpha]_D^{25}$ −1.9 (*c* 0.16, MeOH); UV (MeOH) λ_{max} (logε): 200 (3.25), 270 (2.90) nm; ECD (*c* 2.02 × 10^{-4} mol·L^{-1}, MeOH) λ_{max} ($\Delta\varepsilon$) 215 (2.54), 324 (−0.85) nm; IR (KBr) ν_{max}: 3424, 2958, 1636, 1558, 1386, 1352, 1312, 1207, 1176, 1049, 1026, 1005, 796 cm^{-1}; ^1H (600 MHz, DMSO-d_6) and ^{13}C (150 MHz, DMSO-d_6) NMR, Tables 2 and S6; ESI-MS *m/z* 247.1 [M − H]$^-$; HR-ESI(−)-MS *m/z* 247.0991 [M − H]$^-$ (Calcd. for $C_{14}H_{15}O_4$, 247.0976).

Penicipenoid G (**7**): colorless amorphous solid; $[\alpha]_D^{25}$ +248.0 (*c* 0.09, MeOH); UV (MeOH) λ_{max} (logε): 220 (2.93) nm; ECD (*c* 6.08 × 10^{-4} mol·L^{-1}, MeOH) λ_{max} ($\Delta\varepsilon$) 226 (+32.1) nm; IR (KBr) ν_{max}: 3354, 2956, 2928, 1740, 1559, 1436, 1412, 1368, 1271, 1014, 826, 778, 738 cm^{-1}; ^1H (600 MHz, DMSO-d_6) and ^{13}C (150 MHz, DMSO-d_6) NMR, Tables 2 and S7; ESI-MS *m/z* 295.1 [M − H]$^-$; HR-ESI(−)-MS *m/z* 295.1572 [M − H]$^-$ (Calcd. for $C_{16}H_{23}O_5$, 295.1551).

4.4. X-ray crystallographic analysis

Crystals suitable for X-ray diffraction were obtained for compounds **1**–**4** by vapor diffusion using MeOH and acetone/MeOH (1∶1, *V*/*V*), respectively. Data collection was performed on a Bruker APEX-II CCD diffractometer equipped with graphite-monochromated Cu Kα radiation (λ = 1.541 78 Å) at temperatures of 150, 295(2), 173(2), and 150 K, respectively. Structures were solved by direct methods using SHELXS-97 and refined by full-matrix least-squares on F^2. Crystallographic data have been deposited with the Cambridge Crystallographic Data Center (CCDC) under deposition numbers CCDC 2354542 (**1**), CCDC 2354543 (**2**), CCDC 2354544 (**3**), and CCDC 2354577 (**4**). These data can be accessed free of charge from the CCDC, 12 Union Road, Cambridge CB2 1EZ, UK (tel: (+44) 1223-336-408; fax: (+44) 1223-336-033; e-mail: deposit@CCDC.cam.ac.uk).

*X-ray crystallographic data of penicipenoid A (**1**)*. Yellowish needles, $C_{15}H_{20}O_4$, *Mr* = 264.31, orthorhombic, space group $P2_12_12_1$, *a* = 6.0477(2) Å, *b* = 6.8111(3) Å, *c* = 32.4408(14) Å, α = 90°, β = 90°, γ = 90°, *V* = 1336.29(9) $Å^3$, *T* = 150 K, *Z* = 4, *Dx* = 1.314 mg/m^3, μ(Cu Kα) = 0.772 mm^{-1}, *F*(000) = 568.0, crystal size 0.15 × 0.08 × 0.05 mm^3, 25403 reflections measured (5.448° ≤ 2Θ ≤ 149.028°), 2745 unique (R_{int} = 0.0672, R_{sigma} = 0.0321), all used in calculations. The final R_1 = 0.0311 ($I > 2\sigma(I)$), wR_2 = 0.0805 ($I > 2\sigma(I)$), R_1 = 0.0322 (all data), wR_2 = 0.0815 (all data), *S* = 1.041. The Flack parameter was −0.01(7).

*X-ray crystallographic data of penicipenoid B (**2**)*. Colorless needles, $C_{15}H_{21}ClO_4{\cdot}H_2O$, *Mr* = 318.78, monoclinic, space group $P2_1$, *a* = 6.6202(3) Å, *b* = 8.9129(3) Å, *c* = 13.9435(6) Å, α = 90°, β = 94.122(2)°, γ = 90°, *V* = 820.61(6) $Å^3$, *T* = 295 (2) K, *Z* = 2, *Dx* = 1.290 mg/m^3, μ(Cu Kα) = 2.224 mm^{-1}, *F*(000) = 340.0, crystal size 0.16 × 0.140 × 0.120 mm^3, 11808 reflections measured (5.896° ≤ 2Θ ≤ 68.360°), 2966 unique (R_{int} = 0.0444), all used in calculations. The final R_1 = 0.0388 ($I > 2\sigma(I)$), wR_2 = 0.1063 ($I > 2\sigma(I)$), R_1 = 0.0417 (all data), wR_2 = 0.1094 (all data), *S* = 1.091. The Flack parameter was 0.103(10).

*X-ray crystallographic data of penicipenoid C (**3**)*. Colorless needles, $C_{15}H_{21}ClO_4{\cdot}H_2O$, *Mr* = 320.80, monoclinic, space group $P2_1$, *a* = 11.7528(18) Å, *b* = 9.0755(13) Å, *c* = 15.091(2) Å, α = 90°, β = 92.040(8)°, γ = 90°, *V* = 1608.6(4) $Å^3$, *T* = 173 (2) K, *Z* = 4, *Dx* = 1.325 mg·m^{-3}, *F*(000) = 688.0, μ(Cu Kα) = 2.269 mm^{-1}, crystal size 0.16 × 0.140 × 0.120 mm^3, 32590 reflections measured (2.930° ≤ 2Θ ≤ 68.818°), 5862 unique (R_{int} = 0.1142), all used in calculations. The final R_1 = 0.0674 ($I > 2\sigma(I)$), wR_2 = 0.1681 ($I > 2\sigma(I)$), R_1 = 0.0947 (all data), wR_2 = 0.1919 (all data), *S* = 1.040. The Flack parameter was 0.071(17).

*X-ray crystallographic data of penicipenoid D (**4**)*. Colorless needles, $C_{15}H_{16}O_4$, *Mr* = 260.28, orthorhombic, $C222_1$, *a* = 6.8417(2) Å, *b* = 19.4943(7) Å, *c* = 39.3834(15) Å, α = 90°, β = 90°, γ = 90°, *V* = 5252.7(3) $Å^3$, *T* = 150 K, *Z* = 16, *Dx* = 1.316 mg/m^3, *F*(000) = 2208.0, μ(Cu Kα) = 0.784 mm^{-1}, crystal size 0.12 × 0.04 × 0.03 mm^3, 27431 reflections measured (4.488° ≤ 2Θ ≤ 149.142°), 5257 unique (R_{int} = 0.1031, R_{sigma} = 0.0654), all used in calculations. The final R_1 = 0.0511 ($I > 2\sigma(I)$), wR_2 = 0.1252 ($I > 2\sigma(I)$), R_1 = 0.0594 (all data), wR_2 = 0.1352 (all data), *S* = 1.084. The Flack parameter was 0.10(14).

4.5. ECD calculations

Conformational analyses were performed *via* random search in Spartan 10 using the MMFF force field with an energy cutoff of 3.0 kcal·mol^{-1} [27]. The lowest-energy conformers for compounds **1**–**7** were identified. These conformers were re-optimized using density functional theory (DFT) at the B3LYP/6-31 +G(d, p) level in the gas phase with the GAUSSIAN 09 program [28]. Time-dependent DFT (TDDFT) calculations at the B3LYP/DGDZVP level in MeOH were used to compute the energies, oscillator strengths, and rotational strengths (velocity gauge) of the first 60 electronic excitations. The ECD spectra were simulated using overlapping Gaussian functions (half-bandwidth at 1/e peak height, sigma = 0.32 for all) [29,30]. Final spectra were generated by averaging the simulated spectra of individual conformers according to Boltzmann distribution based on their relative Gibbs free energies (ΔG) [31]. Comparison of experimental and calculated spectra enabled assignment of the absolute configurations of **1**–**7** , as illustrated in Fig. 4 and Figures S11, S22, S33, and S44 (Supporting Information).

4.6. Zebrafish maintenance and embryo handling

Adult zebrafish were maintained at 28 °C under a 14 h light/10 h dark cycle with continuous freshwater supply, aeration, and feeding. Embryos were collected within 30 min after natural spawning and cultured in aquarium systems. Embryos were used within 24 h post-fertilization. All procedures were conducted in accordance with standard ethical guidelines and approved by the Ethics Committee of the Biology Institute of Shandong Academy of Science.

4.7. Antioxidant assay in zebrafish embryos

MTZ treatment induces excessive reactive oxygen species (ROS) production, leading to a significant reduction in FS on the skin of Tg (*krt4:NTR-hKikGR*)^{cy17} zebrafish. Incubation with antioxidants increases the number of FS, allowing evaluation of ROS scavenging activity based on changes in FS count compared to MTZ-treated controls. The *in vivo* anti-oxidant activity of compounds **1**–**17** was assessed using previously described methods with minor modifications in the transgenic line Tg (*krt4:NTR-hKikGR*)^{cy17} [32–34]. Twenty-four-hour-old embryos were placed in 24-well plates (10 embryos/well) and incubated with 2 mL of 10 mmol·L^{-1} MTZ (dissolved in fish water) and test compounds for

24 h at 28 °C. Controls included fish water without MTZ or compounds (vehicle control), MTZ without compounds (negative control), and vitamin C (positive control). After incubation, embryos were anesthetized with tricaine (0.16%, *W/V*) and imaged using an FSX100 Bio Imaging Navigator. Fluorescence spots were quantified using ImagePro-Plus software. The percentage of *in vivo* anti-oxidant activity was calculated as follows:

$$\text{Antioxidant activity}(\%) = \{(\text{FSs} - \text{FSnc})/(\text{FSvc} - \text{FSnc})\} \times 100$$

where FSs denotes the number of fluorescence spots in treated samples, FSnc in the negative control, and FSvc in the vehicle control.

4.8. Anti-inflammatory assay in zebrafish embryos

Transgenic zebrafish Tg (zlyz-EGFP), which express EGFP in macrophages, were used in this study. Healthy larvae at 72 hpf were allocated to 24-well plates (n = 10/well) in 2 mL of embryo medium and divided into six groups: control (fresh fish water), model (10 μmol·L^{-1} $CuSO_4$), positive drug (10 μmol·L^{-1} indomethacin, Solarbio, China), and three test groups (10 μmol·L^{-1} $CuSO_4$ plus 10, 20, or 40 μmol·L^{-1} compound). Compounds were pre-incubated for 2 h, followed by addition of $CuSO_4$ (Sigma Aldrich, St. Louis, MO, USA) and incubation for 1 h. All experiments were performed in triplicate. Larvae were photographed using a fluorescence microscope (AXIO, Zoom.V16), and macrophage counts were determined using Image-Pro Plus software.

Funding

This work was supported by Shanghai Municipal Science and Technology Major Project, the National Key Research and Development Program of China (Nos. 2022YFC2804100 and 2020YFA0509204), the National Natural Science Foundation of China (Nos. 82473795, U24A20808, 82022068, 82173730 and 22137006), and the Innovative Research Team of High-Level Local Universities in Shanghai (SHSMUZDCX20212702).

Supporting information

Supplementary data associated with this article can be requested by sending E-mail to the corresponding authors.

Declaration of competing interest

These authors have no conflict of interest to declare.

References

1 Paul VJ, Freeman CJ, Agarwal V. Chemical ecology of marine sponges: new opportunities through "-omics". *Integr Comp Biol*. 2019;59:765-776. https://doi.org/10.1093/icb/icz014.
2 Moreno-Pino M, Manrique-De-La-Cuba MF, López-Rodríguez M, et al. Unveiling microbial guilds and symbiotic relationships in Antarctic sponge microbiomes. *Sci Rep*. 2024;14(1):6371. https://doi.org/10.1038/s41598-024-56480-w.
3 Liu Y, Ding LJ, Shi YT, et al. Molecular networking-driven discovery of antibacterial perinadines, new tetracyclic alkaloids from the marine sponge-derived fungus *Aspergillus* sp. *ACS Omega*. 2022;7(11):9909-9916. https://doi.org/10.1021/acsomega.2c00402.s001.
4 Zhou GL, Sun CX, Hou XW, et al. Ascandinines A–D, indole diterpenoids, from the sponge-derived fungus *Aspergillus candidus* HDN15-152. *J Org Chem*. 2021;86(3):2431-2436. https://doi.org/10.1021/acs.joc.0c02575.
5 Guo XW, Yu ZQ, Xi J, et al. Isolation and identification of novel antioxidant polyketides from an endophytic fungus *Ophiobolus cirsii* LZU-1509. *J Agric Food Chem*. 2023;71(3):1593-1606. https://doi.org/10.1021/acs.jafc.2c07386.s001.
6 Cho Y, Park KH, Kim E, et al. Talaromides A–C, bioactive cyclic heptapeptides from *Talaromyces siglerae* isolated from a marine sponge. *J Nat Prod*. 2024;87(4):1230-1234. https://doi.org/10.1021/acs.jnatprod.3c01227.
7 Zhang P, Bao B, Dang HT, et al. Anti-inflammatory sesquiterpenoids from a sponge-derived fungus *Acremonium* sp. *J Nat Prod*. 2009;72(2):270-275. https://doi.org/10.1021/np8006793.
8 Hao XM, Li SS, Li JR, et al. Acremosides A–G, sugar alcohol-conjugated acyclic sesquiterpenes from a sponge-derived *Acremonium* species. *J Nat Prod*. 2024;87(4):1059–1066. https://doi.org/10.1021/acs.jnatprod.4c00015.
9 Yang W, Tian S, Du YF, et al. Genome mining of the marine-derived fungus *Trichoderma erinaceum* F1-1 unearths bergamotene-type sesquiterpenoids. *J Nat Prod*. 2024;87(12):2746-2756. https://doi.org/10.1021/acs.jnatprod.4c00905.
10 Zhang B, Zhang T, Xu JZ, et al. Marine sponge-associated fungi as potential novel bioactive natural product sources for drug discovery: a review. *Mini Rev Med Chem*. 2020;20(19):1966-2010. https://doi.org/10.2174/1389557520666200826123248.
11 Liu H, Edrada-Ebel RA, Ebel R, et al. Drimane sesquiterpenoids from the fungus *Aspergillus ustus* isolated from the marine sponge *Suberites domuncula*. *J Nat Prod*. 2009;72(9):1585-1588. https://doi.org/10.1021/np900220r.
12 Julianti E, Oh H, Jang KH, et al. Acremostrictin, a highly oxygenated metabolite from the marine fungus *Acremonium strictum*. *J Nat Prod*. 2011;74(12):2592-2594. https://doi.org/10.1021/np200707y.
13 Dai Q, Zhang FL, Feng T. Sesquiterpenoids specially produced by fungi: structures, biological activities, chemical and biosynthesis (2015–2020). *J Fungi*. 2021;7(12):1026. https://doi.org/10.3390/jof7121026.
14 Bi X, Xu WB, Yao YM, et al. Total syntheses of a family of cadinane sesquiterpenes. *J Org Chem*. 2018;83(10):5825-5828. https://doi.org/10.1021/acs.joc.8b00505.
15 González-Hernández RA, Valdez-Cruz NA, Macías-Rubalcava ML, et al. Overview of fungal terpene synthases and their regulation. *World J Microbiol Biotechnol*. 2023;39(7):194. https://doi.org/10.1007/s11274-023-03635-y.
16 Cui J, Shang RY, Sun M, et al. Trichodermaloids A–C, cadinane sesquiterpenes from a marine sponge symbiotic *Trichoderma* sp. SM16 fungus. *Chem Biodivers*. 2020:17(4):e2000036. https://doi.org/10.1002/cbdv.202000036.
17 Shang RY, Cui J, Li JX, et al. Nigerin and ochracenes J–L, new sesquiterpenoids from the marine sponge symbiotic fungus *Aspergillus* niger. *Tetrahedron*. 2022;104:132599. https://doi.org/10.1016/j.tet.2021.132599.
18 L Y, Jian JY, Xu F, et al. Five new terpenoids from *Viburnum odoratissimum* var. *sessiliflorum*. *Chin J Nat Med*. 2023;21(4):298-307. https://doi.org/10.1016/s1875-5364(23)60438-8.
19 Wang M, Li H, HU BT, et al. Anti-inflammatory germacrane-type sesquiterpene lactones from *Vernonia sylvatica*. *Chin J Nat Med*. 2024;22(6):568-576. https://doi.org/10.1016/s1875-5364(24)60656-4.
20 Li J, Meng X, Yin CY, et al. Antimalarial and neuroprotective *ent*-abietane diterpenoids from the aerial parts of *Phlogacanthus curviflorus*. *Chin J Nat Med*. 2023,21(8):619-630. https://doi.org/10.1016/s1875-5364(23)60464-9.
21 Yaosanit W, Rukachaisirikul V, Phongpaichit S, et al. Sesquiterpenes from the soil-derived fungus *Trichoderma citrinoviride* PSU-SPSF346. *Beilstein J Org Chem*. 2022;18(1):479-485. https://doi.org/10.3762/bjoc.18.50.
22 Liu Z, Zhao JY, Sun SF, et al. Sesquiterpenes from an endophytic *Aspergillus flavus*. *J Nat Prod*. 2019;82(5):1063-1071. https://doi.org/10.1021/acs.jnatprod.8b01084.s001.
23 Song YP, Shi XS, Wang BG, et al. Cadinane and carotane derivatives from the marine algicolous fungus *Trichoderma virens* RR-dl-6-8. *Fitoterapia*. 2020;146:104715. https://doi.org/10.1016/j.fitote.2020.104715.
24 Kawashima J, Ito F, Kato T, et al. Antitumor activity of heptelidic acid chlorohydrin. *J Antibiot*. 1994;47(12):1562-1563. https://doi.org/10.7164/antibiotics.47.1562.
25 Liu L, Han JJ, Xu TS, et al. Three new heptelidic acid derivatives from the culture of mushroom *Lentinellus ursinus*. *Nat Prod Bioprospect*. 2018;8(5):355-360. https://doi.org/10.1007/s13659-018-0168-8.
26 Jiao WH, Dewapriya P, Mohamed O, et al. Divirensols: sesquiterpene dimers from the Australian termite nest-derived fungus *Trichoderma virens* CMB-TN16. *J Nat Prod*. 2018;82(1):87-95. https://doi.org/10.1021/acs.jnatprod.8b00746.s001.
27 Spartan 10, Wavefunction Inc. , Irvine, CA. 2010.
28 Frisch MJ, Trucks GW, Schlegel HB, et al. Gaussian 09, Rev. B. 01; Gaussian, Inc. , Wallingford CT, 2010.
29 Wolinski K, Hinton JF, Pulay P. Efficient implementation of the gauge-independent atomic orbital method for NMR chemical shift calculations. *J Am Chem Soc*. 1990;112(23):8251-8260. https://doi.org/10.1021/ja00179a005.
30 Grimblat N, Zanardi MM, Sarotti AM. Beyond DP4: an improved probability for the stereochemical assignment of isomeric compounds using quantum chemical calculations of NMR shifts. *J Org Chem*. 2015;80(24):12526-12534. https://doi.org/10.1021/acs.joc.5b02396.
31 Stephens PJ, Harada N. ECD cotton effect approximated by the Gaussian curve and other methods. *Chirality*. 2010;22(2):229-233. https://doi.org/10.1002/chir.20733.
32 Li QG, Chu J, Chen XQ, et al. Study on the antioxidant activity evaluation of Jujube (*Ziziphus*) leaf flavonoids *in vitro* and zebrafish (*Danio rerio*) with fluorescent skin. *Sci Technol Food Ind*. 2014;35(5):58-61. https://doi.org/10.13386/j.issn1002-0306.2014.05.071.
33 Chen CF, Chu CY, Chen TH, et al. Establishment of a transgenic zebrafish line for superficial skin ablation and functional validation of apoptosis modulators *in vivo*. *PLoS One*. 2011;6(5):e20654. https://doi.org/10.1371/journal.pone.0020654.
34 Zhang SS, Han LW, Shi YP, et al. Two novel multi-functional peptides from meat and visceral mass of marine snail *Neptunea arthritica cumingii* and their activities *in vitro* and *in vivo*. *Mar Drugs*. 2018;16(12):473. https://doi.org/10.3390/md16120473.